Non-Linear Dispersion of Gamma Dose-Rates and Natural Radionuclides in the Coastal Environments of Unumherin Community in Niger Delta

Omeje Maxwell (maxwell.omeje@covenantuniversity.edu.ng)
Covenant University

Godfrey Usaka Aimua
Covenant University College of Science and Technology

Olusegun Oladotun Adewoyin
Covenant University College of Science and Technology

Joel Emmanuel Sunday
Anchor University Lagos Faculty of Science and Science Education

Muyiwa Michael Orosun
University of Ilorin Faculty of Science

Usikalu Rachael Mojisola
Covenant University College of Science and Technology

Omonhinmin Asotie Conrad
Covenant University College of Science and Technology

Andrew Oha Ifeanyi
University of Nigeria Faculty of Physical Sciences

Benjamin Nnamdi Ekwueme
University of Nigeria Faculty of Engineering

Michael Nwankwo Chukwuma
Covenant University College of Science and Technology

Omeje Uchechukwu Anne
University of Lagos College of Medicine

Research Article

Keywords: Gamma Spectroscopy, Catfish, Niger Delta, Radiological, Cancer Risk, Sediments

Posted Date: August 25th, 2022

DOI: https://doi.org/10.21203/rs.3.rs-1961567/v1

Abstract

The gamma dose rates and the activity concentrations of Potassium-40, Uranium-238, and Thorium-232 in the study area were carried out using calibrated hand-held gamma detector, (RS-125 Gamma-Spectrometer) and NaI (Tl) gamma spectroscopy. The in-situ measurements result of dose rate indicates the hotspot at location 4 with a value of 100 $nGyh^{-1}$, almost twice higher than the recommended limits. The results from NaI (Tl) gamma detector revealed the highest activity concentrations of Potassium-40, Uranium-238, and Thorium-232 to be 288.09, 96.49, 136.12 $Bqkg^{-1}$ for sediments and 257.31, 66.93, 96.57 Bqkg for water, respectively. The highest mean activity concentration of Potassium-40 and Uranium-238 was observed in Catfish with values of 151.87 and 38.00 $Bqkg^{-1}$, whereas the highest value for the activity of Thorium-232 was observed in Tilo Fish with a value of 89.02 Bqkg-1. In comparison, all the observed values are higher than the population-weighted average of 420.00, 32.00, and 45.00 $Bqkg^{-1}$ for Potassium-40, Uranium-238, and Thorium-232 by UNSCEAR. Geologically, this may be attributed to the marine incursion of regional tectonic subsidence during transgression. Statistically, the correlation results confirmed that the enhanced outdoor dose rates at the coastlines environment were caused mainly by Uranium-238, followed by Thorium-232 and then Potassium-40 in magnitude. The mean hazard indices for the samples were observed to be within the world average values recommended by ICRP. The accumulation of radionuclides by fishes may be via ingestion and adsorption to surfaces, which culminate in speciation and mobility of radionuclides, alongside the feeding habits of fishes and other aquatic animals.

1. Introduction

Exposure of humans to ionizing radiation from natural sources is an unavoidable aspect of life here on earth. The principal origin of human exposure to ionizing radiation apart from the radiation coming from the sun through space is terrestrial radiation which emanates predominantly from radionuclides in the uranium and thorium decay series and the non-series potassium-40 (UNSCEAR, 2000). Man's exposure to natural radionuclides has been of concern over the last few decades due to the potential of the radionuclides to induce cancer. The assessment of radioactivity in soil and sediments in the environment is very important for protecting the health of humans and also for the prevention of hazardous effects (Omeje et al., 2020).

The radioactive source in the region of the marine environment could be as a result of natural elements of the Earth's crust or from man-made sources associated with crude oil mining (Abbasi and Mirekhtiary, 2021). Radioactivity measurement is an indicator of the dangers associated with the marine environment from man-made sources such as industrial works and mining (Abbasi et al., 2020). Marine sediments play important role in offering vital information when measuring the environmental and geochemical contamination compared to other potential natural radioactivity sources (Janadeleh et al., 2018b; Janadeleh and Kameli, 2017). Sediments play a dominant role in hydrous radioecology in environmental radioactivity measurements (Abbasi and Mirekhtiary, 2020). These naturally occurring radionuclides

emigrate from the litho-sphere to broader natural ecosystems through the erosion of terrestrial rock and subsequent transport via water, wind, and gravity (Hesham et al., 2021; Abbasi and Mirekhtiary, 2021).

Oil spills, gas flaring, and other human activities of the oil companies have contributed to the massive degradation of marine and land resources. Human exposure to ionizing radiation due to naturally occurring radionuclides has long been a cause of concern (Jibiri & Okeyode, 2012). The radiation from radon and its decay products that sometimes emanate from the soil sediments internally affects the human respiratory tracks (Abbasi 2019a). Evaluation of radioactivity in soil and sediments in an environment is useful for the protection of human health and harmful effects, which is of great interest (Singh & Saxena, 2018). The activity concentrations of radionuclides in the natural ecosystem has resulted in an understanding of the health implications over the past years (Singh & Saxena, 2018). Continuous exposure to even low-level radiation may adversely affect human health Abbasi 2019a. Importantly, to sustain a friendly ecosystem especially in marine environment, an accurate determination of the current radiological hazard risks as highly needed Adegoke et al., 2017). Researchers have mapped out a holistic approach to quantify and evaluate river water quality parameters and their risk exposure to the human and environmental ecosystem (Adegoke et al., 2017).

This study is aimed at assessing the radioactivity level of the marine environments of Unumherin community in Niger Delta, Nigeria and its radiological hazards to the inhabitants.

1.1 Geographical Location and the Geology of the Study Area

The Niger Delta Basin is an extension of the rift basin located in the Niger Delta and the Gulf of Guinea and lies in the southwestern part of the larger tectonic structure called the Benue Trough. It is located on the passive continental margin near the western coast of Nigeria. The volcanic Cameroon line and the passive continental margin bound the other side. It is proven or suspected to have access to Equatorial Guinea, Cameroon and São Tomé, and Príncipe. The basin is complex and carries a very high economic value containing a rich productive hydrocarbon system. The basin is one of the largest subaerial basins in Africa. The sediment fill has a depth ranging between 9 and12 km and is composed of different geologic formations, which indicates the possibility of the formation of the basins. It also indicates the large-scale and regional tectonics of the area, with an extensional basin surrounded by many other basins formed from similar structure processes.

The study area covers two (2) communities in Warri Area in the Niger Delta as shown in Fig. 1. They are Unumherin and Okirigwe communities in Delta State of Nigeria fondly called “Glory of All Lands” and are geographically located between latitudes 4.264825^{o}– 5.414860^{o} North of Equator and between longitudes 5.372116^{o} – 6.727176^{o} East of Greenwich.

The geology of Niger Delta covers about 256,000 km. Initially, it was the older transgressive Paleocene prodelta that was built, which was Delta construction, and proceeded in discreet mini basins (d’Almeida et

al., 2016). These mini basins range in tectonic configuration from extensional through translational to compressional toe-thrust region. The Niger Delta outcropping units are Imo Formation and the Ameki Group. The Ameki group includes the Ameki, Nanka, Nsugbe, and Ogwashi-Asaba formation. The lithostratigraphic sequence of the subsurface units is major transgressive marine Akata shales, the petroliferous paralic Agbada Formation, and the continental Benin Sands (Adegoke et al, 2017; d'Almeida et al., 2016). The crude oil in Niger Delta has a low amount of sulfur, nickel-bearing, light waxy, and nongraded. The location and geology of the study area are shown in Fig. 1.

The delta sequence comprises an upward-coarsening regressive association of the Tertiary clastics of up to 12 km thick. It is divided into three gross lithofacies namely: (i) marine shale and clay stones of unknown thickness at the base (ii) alternations of clay stones, sandstones, and siltstones, of which the percentage increase of sand is upwards (iii) the alluvial sand is on the top. The stratigraphy and the Delta structure are related intimately. Each of the development are being dependent on the interplay existing between the subsidence rates and sediment supply. The most dominant structures of the subsurface are post- and sync- sedimentary lithic normal faults which can affect the main sequence of the delta.

1.2 The Coastline Sediments of Atlantic Coast of Unumherin Community and Ethiope River

The nature of the Atlantic Coast of the Unumherin Community and the Ethiope river sediments shows some parts where communities have access to the Atlantic Ocean and Ethiope River for fishing and fetching water for domestic purposes (Jibiri & Okeyode, 2017). They are parallel to the coastline sediments of other Atlantic coastal regions of Escravos, Forcados, Burutu, and Agbaro which are located about some kilometers away from Unumherin Community and Ethiope River. The deposits from the Atlantic Ocean and Ethiope River comprise mudflats, salt marsh, and inner sandy flats. Within the Ocean and river sub-environments, it cuts across the creeks and the bordering areas. Surface features such as vegetation, an association of different sediments, sedimentary structures, and textures, characterize the sub-environments along the coastal region and rivers. The sediments contain high contents of iron, phosphate, nitrate, and sulfates (Mutiu et al., 2013). The tidal water along the ocean and river decreases its capacity towards the intertidal zone, and this increases the sediments deposits and as well reduces the size of the grains. These processes seem to be modified by the secondary agents caused by waves for rearrangements of the sediments in the study area.

2. Materials And Methods

2.1 In-situ Gamma Spectroscopy Measurements using Super-Spec RS125 Gamma Spectrometer

The In-situ measurement of the background gamma dose rates and the activity concentration of K-40, Th-232, and U-238 was carried out about 1 meter above the ground surface using a Super SPEC RS-125 gamma detector coated with 2.0 cm x 2.0 cm NaI crystal. To accurately measure the levels of

radioactivity going on in the sediment samples, the procedure of Omeje et al., 2020 was adopted. A Portable hand-held radiation detector (Super-SPEC RS-125) from Canadian Geophysical Inc. was used to measure the background gamma dose level in the study area. This instrument is most suitable for detecting naturally occurring radionuclides and dose exposure. The equipment has a high degree of accuracy with probable measurement errors of about ± 5% or uncertainty of ± 5% at energies above 500 keV. In this case, due to the sensitivity of the response at low energies to the individual detectors' characteristics, it can be used below 200 keV. The portable equipment has an incorporated design and direct assay read-out values, and the storage data point with weather protection is easy to use and highly sensitive. At each station, 4 different measurements were taken and the average obtained was used to represent the actual data point for that site. At each point of measurement, the sediment sample was collected for laboratory gamma-ray spectroscopy counting. The background measurement was provided by the assay mode of RS-125 Super SPEC and dose rate data is directly acquired in nGy/h (Omeje et al., 2020). The measured data are stored in an excel sheet with proper coordinates processed, georeferenced, and interpolated using ArcGIS (version 10.8) spatial analysis. Figure 2 presents the result of the ArcGis spatial distribution of dose rate measured in the study area.

2.2 Method of GIS Analysis of Background Dose Rates data Samples Measured in the study area

*T*he spatial distribution of gamma dose rates in the coastal environments was carried out using an interpolated scheme of the inverse distance weighting interpolation function being applied on all the surveyed area. The interpolated functions were used as input to the ArcGIS 10.8. The variables used are 1, output cell size of 30m with the power 2.

2.3 Sample Collection and preparation of soil Sediments, Water, and Fishes for Laboratory Gamma-Ray Spectrometry Measurements

A total number of sixteen (16) samples from sediments, water, and five (5) different species of fish were collected randomly within the selected coastal environments in the Warri Area of the Niger Delta in accordance with IAEA guidelines on the collection of soil samples for analysis (Omeje et al., 2020). They were obtained from the specified areas of the Unumherin Community between February 8 and 14, 2021, and the locations are shown in Fig. 2. A minimum distance of 20 meters was maintained between two sampling points and black polythene bags were used for the packing, taped up and marked according to the location, and together with a designated site code and coordinates of the sample. The samples were scooped at a depth between 10 and 50 cm (vertical distance) using a hand trowel. In the Unumherin Community, fifteen (15) different sediment samples were collected at the stations of the measured in-situ background gamma measurements, and a sample outside the study area was used as a control to sum it up to sixteen (16) sediment samples altogether. The samples were taken to Covenant University Microbiology Laboratory, where macroscopic traces of stones, rubbers, glass, plastic, animal and plant matter, and other large particles were removed to make sure the materials to be analyzed does not

contain such impurities. The samples of sediments and fishes were air-dried at room temperature of about 29 ^{0}C, for 3 days to reduce the mass contribution of water and to prevent any chemical reaction. The dried samples were later crushed using a ball mill to reduce the particle size and subsequently further dried in an electric oven at a temperature of 110 ± 1 ^{0}C for 24 hours to completely remove any remnant moisture and obtained constant weight. Water samples were collected in high-density polyethylene containers at the site which were previously washed in a solution of 10% nitric acid for 15 minutes, followed by repeated rinsing with distilled water and finally rinsing with ultrapure water (resistivity of about 18 M cm^{-1}). The containers used for the collection were kept in sealed polyethylene bags before the collection of samples. To prevent it from contaminating the wall of the container, the water samples were stabilized with 5 ml of nitric acid in each liter of water.

2.4 Sample Preparation/ Calibration of Detector for Gamma Spectroscopy Analysis

The Soil samples were collected into a very clean polythene bag and well labeled to avoid mixing up of samples. The samples were transported to CERT, Ahmadu Bello University, Zaria. The collected samples were dried at ambient temperature until there was no noticeable change in the mass of the sample. The dried samples were carefully crushed, grounded, and pulverized to a powdery form. The powder was passed through a 2mm sieve. Only 200g – 300g of the samples (dry–weight) were utilized for analysis due to the limited space of the detector shield.

To prevent ^{222}Radon from escaping, three different methods were adopted for sealing in each case. The sealing procedure involved coating the internal rim of the lid of the plastic container with Vaseline jelly, filling the lid assembly gap with candle wax to block the gaps between lid and container, and tight-sealing lid-container with adhesive masking tape.

The samples were transferred to radon-impermeable cylindrical plastic containers of uniform size (70mm height by 60mm diameter) after weighing and were sealed for about 30 days. This was done to allow radon and its short-lived progenies to reach secular radioactive equilibrium before gamma measurements. The soil used for referencing was also transferred to a container of the same material and dimensions as were used for the fish samples. A lead-shielded 76 × 76 mm NaI (TI) detector crystal (Model No. 727 series, Canberra Inc.) that is coupled to a Canberra Series 10 plus Multichannel Analyzer (MCA) (Model No.1104) through a preamplifier was used for the radioactivity measurements. It has a resolution (FWHM) of about 8% at energies of about 662.0 keV, which is considered adequate to distinguish the gamma ray energies of interest in this current study. The choice of gamma ray peaks the radionuclides to be used for measurement in this study was made considering the fact that NaI(TI) detector used in this study had a modest energy resolution. This was to ensure that the photons emitted by the radionuclides would only be sufficiently discriminated if their emission probability and their energy were high enough, and the surrounding background continuum low enough. Therefore, the activity concentration of ^{214}Bi (determined from the 1760 keV gamma ray peak) was chosen to provide an estimate of 226Ra (^{238}U) in the samples, while that of the daughter radionuclide 208Ti (determined from

its 2615 keV gamma ray peak) was chosen as an indicator of ^{208}Th (^{232}Th). ^{40}K was determined by measuring the 1460 keV gamma rays emitted during its decay. Detailed information about the gamma-spectrometry procedures can be found in our previous work (Omeje et al., 2020; Orosun et al., 2020). The minimum detectable activity for ^{40}K, ^{238}U, and ^{232}Th were 0.0255, 0.00737, and 0.00737 $Bqkg^{-1}$, respectively. The fish samples were placed on top of the detector symmetrically and measured for 29000 seconds, which was followed by that of water and sediments. The net area under the corresponding peaks in the energy spectrum was computed by subtracting counts due to Compton scattering of higher peaks and other background sources from the total area of the peaks Omeje (Omeje et al., 2020; Orosun et al., 2020).

2.5 Calibration and Efficiency Determinations

The system was calibrated for energy and efficiency. Two calibration point sources were used in calibrating the system, ^{137}Cs and ^{60}Co. The calibrations were done with an amplifier gain that gives 72% energy resolution for the 661.7 keV of Cs-137 and counted for 30 minutes with the spectral lines of Cobalt-60 found to be 1.161 ± 0.02 MeV and 1.325 ± 0.02 MeV.(Graba et al., 2018; Omeje et al., 2020)

.

Table 1
Spectral energy windows used in the Analysis

Isotope	Gamma Energy (keV)	Energy Window (keV)
R-226	1764.0	1620–1820
Th-232	2614.5	2480–2820
K- 40	1460.0	1380–1550

2.6 Estimation of the Radiological Hazard Indices

Absorbed Dose Rate

The absorbed dose rate in the air due to the concentration of the activities of preexisting radionuclides Potassium-40, Uranium-238, and Thorium-232 ($Bqkg^{-1}$) at the coastal regions was estimated using Eq. 1 ; (UNSCEAR, 2020; Graba et al., 2018; Omeje et al., 2020)

$$D\left(nGyh^{-1}\right) = 0.462C_u + 0.604C_{Th} + 0.041C_K$$

,

, 2

where C_K, C_u, and C_{Th} are the activities of Potassium-40, Uranium-238, and Thorium-232 in the study samples, respectively [1,19].

Annual Effective Dose for External Exposures (AED $_{Ext}$)

The effective dose for external exposure received by a member of the public annually was estimated using the dose rates as given in the equations below.

$AED_{outdoor}$ (μSvy^{-1}) = $D_{outdoor}$ (nGyh^{-1}) × 8760h×0.7 (Sv Gy^{-1}) × 0.2×10^{-3}, 2

The dose conversion factor of 0.7 *SvGy*$^{-1}$ and occupancy factor for indoor as 0.8 were adopted [1].

Radium Equivalent Activity Index (Ra $_{eq}$)

The radium equivalent (Ra_{eq}) was calculated using Eq. 3:

$$Ra_{eq} = C_{Ra} + 1.43C_{Th} + 0.077C_{K}, 3$$

where C_{Ra}, C_{Th}, C_K are the radioactivity concentration in Bq kg^{-1} of ^{226}Ra, Thorium-232, and Potassium-40. The average value of the Radium Equivalent Activity Index (Ra_{eq}) is 370 Bq kg^{-1}.[19]

Radiation Hazard Indices:

Excess Lifetime Cancer Risk (ELCR)

The Excess Lifetime Cancer Risk (*ELCR*) was calculated using Eq. 9:

ELCR = AED × DL × RF 9

where *AED is* the Annual Effective Dose, *DL* is the mean life duration (assuming 70 years) and RF is the fatal cancer risk per Sievert assumed to be 0.05 for stochastic effects for the populace (UNSCEAR, 2020; Orosun et al., 2020b; Omeje et al., 2020). The recommended limit for the ELCR is 3.75 x 10^{-3}.

2.7 Statistical Analysis

The Pearson correlation analysis and the descriptive statistical analysis were carried out using **S**tatistical **P**ackage for the **S**ocial **S**ciences (SPSS). The two variables to be tested to ensure that Pearson is checked under Correlation Coefficients and the results were displayed at the output viewer of the SPSS. Similarly, the descriptive statistics were analyzed using descriptive coefficients to give the desired variability of spread samples in the study area

3. Results And Discussion

3.1 In situ Activity concentration using Super-Spec RS125 -Spectrometer

The statistical summary of the results of the *in situ* measured activity concentrations of Uranium-238, Thorium-232, Potassium-40, and the gamma dose rate (*DR*) for the seashores are presented in Table 2 and Figs. 3–6. The results revealed that the activities of the primordial radionuclides were skewed (having almost a symmetric distribution) since most of the measure of the asymmetry of their probability distribution about their means is in the range of -2 and + 2 (Sugandhi et al., 2014; Orosun et al., 2020b). The evaluation of the coefficient of variation (CV) also discloses the variability in the distribution of the concentration of the activities at the polluted coastlines. From the results, most of the activities show high variability.

From Table 2, the lowest values of the activity concentration of Potassium-40, Uranium-238, and Thorium-232 for the study area are 0.00 $Bq\ kg^{-1}$ (below the detection limit), while their corresponding highest values are 331.78, 53.11, and 46.28 $Bqkg^{-1}$, respectively. Interestingly, the highest activities of Uranium-238 and Thorium-232 occur at the same sampling point (i.e. location 9) which may be due to the presence of silicate sand in the sediments and the lowest values of the activities of Potassium-40 and Uranium-238 occur at location 14, which may be attributed to the weather/washing away of major contents of the sediments. These high and low activity concentrations of these primordial radionuclides are evident in the spatial plots using ArcGIS (Figs. 3–6). The high observed values at location 9 call for serious concern since a considerable increase in the concentration of the radionuclides increases the level of the background radiation that can lead to exposure to elevated ionization radiation levels. The estimated mean values of the in-situ measured activities of Potassium-40, Uranium-238, and Thorium-232 are 135.28, 17.29, and 19.94 $Bqkg^{-1}$ respectively. These mean values of the activity concentration of the radionuclides are below 420.00, 32.00, 45.00 $Bqkg^{-1}$ acceptable threshold values for exposure to Potassium-40, Uranium-238, and Thorium-232 respectively, provided by ICRP (1991); IAEA (1996). & UNSCEAR (2000).

Pearson correlation analysis was done to further investigate the connection between these measured radionuclides and the in-situ measured outdoor gamma dose rate. The result of the correlation analysis which is presented in Table 3, were classified according to the correlation coefficient R [15, 19] i.e.

1. $0.7 \leq |R| \leq 1$ indicates a strong correlation;
2. $0.5 \leq |R| \leq 0.7$ suggests a significant correlation;
3. $0.3 \leq |R| \leq 0.5$ reveals a weak correlation; and

$|R| < 0.3$ indicates an insignificant correlation.

A strong correlation exists between Uranium-238 and D_{out} (R = 0.7034), and a significant correlation was observed between Thorium-232 and D_{out} (R = 0.6482) and between Potassium-40 and D_{out} (R = 0.5003). However, an inconsequential correlation was observed to exist between the primordial radionuclides. The correlation results confirm that the enhanced outdoor dose rates at coastal sediments were caused mainly by Uranium-238, followed by Thorium-232 and then Potassium-40 as shown in Table 3

Table 2
The acquired Field Data (In-situ measurements of Uranium-238, Thorium-232, and Potassium-40 activities)

Points	Lat. (North)	Long. (East)	Elev. (m)	^{238}U (Bq/kg)	^{232}Th (Bg/kg)	^{40}K (Bq/kg)
1	5.933108	5.519315	-19	0.00	2.84	71.99
2	5.932997	5.519288	-16	32.11	29.35	331.78
3	5.933073	5.519443	-13	44.46	0.00	84.51
4	5.932915	5.519445	-14	8.65	29.23	319.26
5	5.330450	5.519607	-14	28.41	20.42	131.46
6	5.932897	5.519582	-20	6.16	33.33	131.46
7	5.933080	5.519582	-15	7.41	0.81	3.93
8	5.933045	5.598950	-17	16.10	20.72	134.93
9	5.933015	5.520023	-17	53.11	46.28	37.56
10	5.932983	5.520178	-18	7.41	28.42	12.52
11	5.932855	5.520070	-16	34.58	1.22	325.32
12	5.932740	5.520125	-18	20.99	13.80	316.13
13	5.932993	5.520312	-26	0.00	38.98	75.12
14	5.933052	5.520335	-21	0.00	26.39	0.00
15	5.932777	5.520295	-21	0.00	7.31	53.21

Table 3
Pearson correlation for the primordial radionuclides (Potassium-40, Uranium-238, Thorium-232, and D_{out}).

	^{238}U	^{232}Th	^{40}K	D_{out}
^{238}U	1.0000			
^{232}Th	0.0412	1.0000		
^{40}K	0.2883	0.0436	1.0000	
D_{out}	0.7034	0.6482	0.5003	1.0000

3.2 Activities of Potassium-40, Uranium-238, and Thorium-232 in the sediment, water, and fish samples from the coastline using 3 x 3 inch NaI[Tl] Detector.

The statistical summary of the results of the measured activity concentrations of Uranium-238, Thorium-232, *and* Potassium-40 in the sediments, waters, and fishes from the sediment seashores are presented in Tables 3 to 5 and Figs. 7–9. The results revealed similar distribution observed in the in-situ measurements i.e. the activities of the primordial radionuclides were skewed (having a symmetric distribution) since most of the measure of the asymmetry of their probability distribution about their means is in the range of -2 and + 2 (Sugandhi et al., 2014).

From Tables 4 and 5, the minimum values of the activity concentration of Potassium-40, Uranium-238, and Thorium-232 for sediments and waters from the study area are 102.23, 54.24, 47.65 $Bqkg^{-1}$ and 126.71, 39.43, 60.24 BqL^{-1}, respectively, while their highest values are 288.09, 96.49, 136.12 $Bqkg^{-1}$ and 257.307, 66.93, 96.57 BqL^{-1}, respectively. This high radioactivity level in water might be triggered by the chemistry of the hydrocarbon/oil spillage in the aqueous phase or due to the high contents of the drilling fluids used in oil explorations in the region. The estimated mean values of these measured activities of Potassium-40, Uranium-238, and Thorium-232 for the sediment and water are 200.07, 70.02, 94.88 $Bqkg^{-1}$, and 193.73, 52.59, 82.00 BqL^{-1} respectively. The mean values of the activity concentration of Potassium-40 for both sediment and water were observed to be below the recommended level of 420.00 $Bqkg^{-1}$. Whereas the average activities of Uranium-238 and Thorium-232 for both sediment and water were detected to be way above their corresponding world average values of 32.00, and 45.00 $Bqkg^{-1}$ respectively, provided by [20], (ICRP, 1991; IAEA,1996 & UNSCEAR, 2000). These differences may be a result of sediment deposition underlying the study area which is controlled by the geology of the area. The activity concentrations of these primordial radionuclides are displayed in Figs. 7 and 8.

From Table 6 and Fig. 9, the mean concentration of the primordial radionuclides varies from one species of fish to another. The highest mean concentrations Potassium-40 and Uranium-238 were observed in Catfish with 151.87 and 38.00 $Bqkg^{-1}$, respectively. Whereas, the highest mean activities of Thorium-232 were observed in Tilo with 89.02 $Bqkg^{-1}$. Differences in the eating habits and metabolism of the fishes are believed to be the cause of these variations. It is well known that metabolic activity and feeding habits are one of the most important factors that play an important role in toxic elements accumulation in aquatic animals (Orosun et al., 2016).

Table 4
Activities of Potassium-40, Uranium-238, and Thorium-232 in the sediment samples from the coastline using 3 x 3 inch NaI[Tl] Gamma Spectroscopy Analysis

S/No.	Sample ID	Potassium-40 ($Bqkg^{-1}$)	Uranium-238 ($Bqkg^{-1}$)	Thorium-232 ($Bqkg^{-1}$)
1	S1	224.43 ± 1.3	83.47 ± 4.8	105.77 ± 2.3
2	S2	242.24 ± 1.5	75.00 ± 0.4	47.66 ± 2.0
3	S4	106.13 ± 1.9	54.90 ± 2.1	76.24 ± 1.0
4	S3	184.53 ± 1.3	60.89 ± 1.1	109.46 ± 0.8
5	S5	252.70 ± 1.9	80.63 ± 1.5	84.69 ± 1.3
6	S7	194.72 ± 2.6	72.76 ± 2.7	79.58 ± 0.1
7	S9	137.61 ± 2.4	76.24 ± 0.1	136.12 ± 0.5
8	S8	259.02 ± 1.4	71.84 ± 2.0	76.59 ± 2.8
9	S6	239.93 ± 2.3	58.25 ± 1.9	103.21 ± 2.3
10	S11	280.31 ± 0.9	96.50 ± 1.2	104.86 ± 1.9
11	S10	288.09 ± 2.5	57.30 ± 1.6	92.09 ± 2.8
12	S12	116.14 ± 1.2	59.24 ± 0.1	132.12 ± 0.2
13	S14	182.72 ± 3.0	65.52 ± 1.8	66.72 ± 1.2
14	S13	190.21 ± 1.5	54.25 ± 1.6	103.21 ± 1.3
15	S15	102.23 ± 1.0	83.44 ± 1.0	104.87 ± 1.9
16	S_Control	91.34 ± 0.1	46.23 ± 0.0	37.09 ± 0.1
	Min	102.23	54.25	47.66
	Max	288.09	96.50	136.12
	Mean	200.07	70.02	94.88
	Standard Error	16.10	3.27	6.10
	Median	194.72	71.84	103.21
	Mode	#N/A	#N/A	103.21
	STDV	62.34	12.67	23.61
	Variance	3885.89	160.44	557.71
	Kurtosis	-1.14	-0.56	0.05

S/No.	Sample ID	Potassium-40 ($Bqkg^{-1}$)	Uranium-238 ($Bqkg^{-1}$)	Thorium-232 ($Bqkg^{-1}$)
	Skewness	-0.31	0.48	-0.10
	Range	185.86	42.25	88.47

Table 5
Activities of Potassium-40, Uranium-238, and Thorium-232 in the water samples from the coastline using 3 x 3 inch NaI[Tl] Gamma Spectroscopy Analysis

S/No.	Sample ID	Potassium-40 (BqL^{-1})	Uranium-238 (BqL^{-1})	Thorium-232 (BqL^{-1})
1	WS1	154.61 ± 2.8	60.81 ± 2.1	83.55 ± 2.2
2	WS2	158.15 ± 1.6	66.93 ± 1.6	60.24 ± 1.1
3	WS3	257.31 ± 2.1	43.79 ± 2.1	78.95 ± 0.8
4	WS4	203.41 ± 0.5	44.59 ± 1.4	83.12 ± 1.7
5	WS5	135.52 ± 2.5	64.65 ± 2.9	92.67 ± 0.1
6	WS6	135.73 ± 1.7	39.44 ± 0.4	69.36 ± 3.1
7	WS7	200.09 ± 1.6	50.54 ± 2.1	92.48 ± 1.6
8	WS8	257.31 ± 2.1	63.69 ± 1.1	96.57 ± 2.1
9	WS9	178.85 ± 1.3	56.94 ± 2.4	85.36 ± 2.0
10	WS10	220.25 ± 2.4	50.98 ± 1.9	87.09 ± 3.8
11	WS11	226.42 ± 2.4	57.46 ± 0.9	85.24 ± 0.8
12	WS12	126.71 ± 1.4	45.17 ± 0.6	73.32 ± 3.8
13	WS13	237.30 ± 2.1	52.32 ± 1.1	94.51 ± 2.0
14	WS14	200.00 ± 1.4	48.54 ± 2.0	84.45 ± 1.1
15	WS15	214.24 ± 2.0	42.92 ± 1.8	63.08 ± 3.0
16	WS_Control	123.81 ± 0.1	39.65 ± 1.0	48.13 ± 1.0
	Min	126.71	39.44	60.23
	Max	257.31	66.93	96.57
	Mean	193.73	52.59	82.00
	Standard Error	11.27	2.26	2.87
	Median	200.09	50.98	84.45
	Mode	257.30	#N/A	#N/A
	STDV	43.60	8.75	11.10
	Variance	1900.71	76.48	123.29
	Kurtosis	-1.18	-1.21	-0.30

S/No.	Sample ID	Potassium-40 (BqL^{-1})	Uranium-238 (BqL^{-1})	Thorium-232 (BqL^{-1})
	Skewness	-0.14	0.24	-0.73
	Range	130.59	27.49	36.33

Table 6
Activities of Potassium-40, Uranium-238, and Thorium-232 in the Fish samples from the coastline using 3 x 3 inch NaI[Tl] Gamma Spectroscopy Analysis

S/No.	Sample ID	Potassium-40 ($Bqkg^{-1}$)	Uranium-238 ($Bqkg^{-1}$)	Thorium-232 ($Bqkg^{-1}$)
1	Cat Fish	151.87 ± 0.1	37.10 ± 1.4	65.51 ± 0.8
2	Tilapia	149.78 ± 0.8	30.61 ± 1.1	50.72 ± 1.3
3	Gold Fish	101.57 ± 2.3	24.25 ± 2.9	80.37 ± 1.2
4	Tilo	135.41 ± 2.4	18.38 ± 1.6	89.02 ± 1.6
5	Til-1	104.79 ± 1.3	37.32 ± 2.0	59.77 ± 1.9

3.3 Evaluation of the in-situ radiological hazard indices for the coastal Environment.

The radiological hazard indices were estimated to evaluate the radiological risks for the coastal environment. The hazards parameters calculated are presented in Table 7. While the outdoor absorbed dose (D_{out}) rate was obtained *in-situ* using the RS-125 gamma spectrometer, the indoor absorbed dose rate (D_{in}) was estimated using Eq. 2 and the resulting values were used to evaluate the annual effective doses. The maximum and minimum values of the outdoor and indoor absorbed dose rate were observed in location 9 with 54.03 and 102.77 nGy/h and location 1 with 4.07 and 8.02 nGy/h respectively. Expectedly, this location 9 corresponds to the location of high activities of Uranium-238 and Thorium-232. This means that the risk associated with exposure to ionizing radiation is high for this location. The mean values of the outdoor and indoor absorbed dose rate are 25.58 and 48.88 nGy/h respectively. These mean values are considerably lower than the world average value of 59.00 and 84.00 nGy/h provided by UNSCEAR, 2000. Similarly, the highest and lowest outdoor and indoor annual effective dose values were observed in location 9 with 0.07 and 0.50 mSv/y, and location 1 with 0.01 and 0.04 mSv/y respectively. The mean values calculated for the outdoor and indoor annual effective doses (0.03 and 0.24 mSv/y, respectively) are within the world average value of 0.07 and 0.41 mSv/h for outdoor and indoor exposures respectively.

The estimated values for the *ELCR* corroborated our earlier findings with location 9 and Location recording the maximum and minimum values respectively. Fortunately, the mean values estimated for all the hazard indices are within their corresponding recommended limits.

Table 7
In-situ Radiological hazard indices for the study area.

	Din ($nGyh^{-1}$)	D_{out} ($nGyh^{-1}$)	AED ($mSvy^{-1}$)	Ra_{eq} ($Bqkg^{-1}$)	H_{ext}	ELCR
1	8.89	4.67	0.01	9.61	0.03	0.15
2	88.37	46.17	0.06	99.63	0.27	1.52
3	47.66	24.01	0.03	50.97	0.14	0.82
4	65.65	34.74	0.04	75.03	0.20	1.13
5	59.11	30.85	0.04	67.73	0.18	1.01
6	52.86	28.37	0.03	63.96	0.17	0.91
7	8.02	4.07	0.00	8.87	0.02	0.14
8	48.35	25.46	0.03	56.07	0.15	0.83
9	102.77	54.03	0.07	122.18	0.33	1.76
10	39.08	21.10	0.03	49.01	0.13	0.67
11	59.18	30.05	0.04	61.37	0.17	1.02
12	59.79	31.00	0.04	65.08	0.18	1.03
13	48.88	26.62	0.03	61.52	0.17	0.84
14	29.03	15.94	0.02	37.74	0.10	0.50
15	12.30	6.60	0.01	14.55	0.04	0.21
Min	8.02	4.07	0.01	8.87	0.02	0.14
Max	102.77	54.03	0.07	122.18	0.33	1.76
Mean	48.66	25.58	0.03	56.22	0.15	0.84
Std Err	6.97	3.64	0.00	8.01	0.02	0.12
Median	48.88	26.62	0.03	61.37	0.17	0.84
Std Dev	26.98	14.09	0.02	31.04	0.08	0.46
Variance	727.78	198.48	0.00	963.33	0.01	0.21
Kurt	0.03	0.10	0.10	0.44	0.43	0.03
Skew	0.18	0.18	0.18	0.25	0.25	0.18
CV	55.44	55.08	55.08	55.21	55.17	55.44
Range	94.75	49.96	0.06	113.31	0.31	1.63

3.4 Evaluation of the radiological hazard indices for the sediments, waters, and fishes from the study area using the Laboratory Gamma Spectroscopy Analysis data

The estimated radiological indices are provided in Tables 8–10, respectively for the sediments, waters, and fishes from the coastal environment. The average values of the outdoor and indoor absorbed dose rates estimated for the sediments are 97.86 and 184.79 nGy/h, respectively. Similarly, the highest and lowest outdoor and indoor annual effective doses are 0.09 and 0.69 mSv/y, respectively. The estimated mean values of the outdoor and indoor annual effective doses are also higher than the world average value of 0.07 and 0.41 mSv/y for outdoor and indoor exposures respectively. The mean AED_{ing}, which is a result of ingestion of the radionuclides in the water is 0.2538 mSv/y. However, this mean value is less than the 1.00 mSv/y recommended by ICRP 1991 & UNSCEAR, 2000. The estimated mean values of AED *and the ELCR* follow suit and corroborated our earlier findings for water and AED *and ELCR for* fish. Fortunately, the estimated average values for the hazard indices of the fishes are within their respective recommended limits.

Table 8
Radiological hazard indices for sediments and Water from the study area

Sediments						Water	
Points	D_{in} ($nGyh^{-1}$)	D_{out} ($nGyh^{-1}$)	Ra_{eq} $Bqkg^{-1}$	AED ($mSvy^{-1}$)	ELCR (x 10^{-3})	AED_{ing} ($mSvy^{-1}$)	ELCR (x 10^{-3})
S1	211.09	111.65	252.00	0.14	3.62	0.2593	0.9074
S2	140.80	73.36	161.80	0.09	2.42	0.2019	0.7068
S4	142.86	75.76	172.10	0.09	2.45	0.2458	0.8604
S3	191.20	101.82	231.64	0.12	3.28	0.2533	0.8865
S5	187.56	98.77	221.20	0.12	3.22	0.2836	0.9926
S7	170.06	89.67	201.56	0.11	2.92	0.2101	0.7354
S9	230.88	123.08	281.49	0.15	3.96	0.2804	0.9816
S8	171.07	90.07	201.32	0.11	2.94	0.3018	1.0563
S6	186.32	99.09	224.33	0.12	3.20	0.2637	0.9229
S11	226.55	119.41	268.04	0.15	3.89	0.2681	0.9382
S10	177.05	93.90	211.16	0.12	3.04	0.2670	0.9344
S12	209.13	111.93	257.12	0.14	3.59	0.2227	0.7795
S14	148.29	78.06	175.01	0.10	2.55	0.2893	1.0124
S13	178.66	95.20	216.49	0.12	3.07	0.2585	0.9048
S15	200.29	106.08	241.26	0.13	3.44	0.2010	0.7036
S_Control	90.63	47.50	106.30	0.06	1.56	0.1541	0.5394
Min	140.80	73.36	161.80	0.09	2.42	0.2010	0.7036
Max	230.88	123.08	281.49	0.15	3.96	0.3018	1.0563
Mean	184.79	97.86	221.10	0.12	3.17	0.2538	0.8882

Table 10
Radiological hazard indices for the Fishes from the study area.

Sample Type	AED_{ing} ($mSvy^{-1}$)	ELCR ($x\ 10^{-3}$)
Cat Fish	0.2005	0.7017
Tilapia	0.1581	0.5533
Gold Fish	0.2286	0.8002
Tilo	0.2505	0.8768
Til-I	0.1819	0.6366

4. Conclusions

This study reported the in-situ measurements and laboratory activity concentrations of Potassium-40, Uranium-238, Thorium-232, and the outdoor dose rate of the study area in Niger-Delta areas of Nigeria. The in-situ measurements were consolidated with laboratory analysis of sediments, water, and fishes from the same coastal region. The results revealed varying activities of the preexisting radionuclides (Potassium-40, Uranium-238, and Thorium-232) with average values within the acceptable limits for the in-situ measurements. However, values within the world average values for the radionuclides recorded in the measured samples. Similarly, the radiation impact assessments reveal values that are mostly within the world average values for the in-situ and as well in sediments and water samples. Significantly, the estimated mean values of all the hazard indices for the measured samples are within their respective worldwide population weighed mean concentration. This study recommended further research on soil sediments and marine water microbial and geochemical analysis to derive a comprehensive conclusion on what could be the main cause of death of fishes.

Declarations

Author Contributions: AGU, OM, AOO, and JES, conceived and designed the research work. MMO, AGU, and UMR, collect the data and wrote the paper. MMO, GN, and MAS performed the risks analysis and final compilation of the work.

Funding: The authors did not receive funding for this research.

Institutional Review Board Statement: Not applicable.

Informed Consent Statement: Not applicable.

Data Availability Statement: The data supporting the findings of this study are available on request from the corresponding author.

Acknowledgments: Authors would like to thank the Covenant University Center for Research, Innovation, and Discovery (CUCRID) for providing enabling Environment to execute this research. In addition, we thank the Unumherin Community in Niger Delta for their assistance during the data collection. Finally, we thank the Biotechnology and Radiation Geophysics Research Cluster for their effective contributions in all aspects of this study.

Conflicts of Interest: The authors declare no conflict of interest.

References

1. Abbasi A, Zakaly HMH, Mirekhtiary F (2020) Baseline levels of natural radionuclides concentration in sediments east coastline of North Cyprus. Mar Pollut Bull 161. https://doi.org/10.1016/j.marpolbul.2020.111793
2. Abbasi A, Zakaly HMH, Badawi A (2021) The anthropogenic radiotoxic element of 137Cs accumulate to biota in the Mediterranean Sea. Mar Pollut Bull 164:112043. https://doi.org/10.1016/j.marpolbul.2021.112043
3. Abbasi A (2019a) ^{210} Pb and ^{137} Cs based techniques for the estimation of sediment chronologies and sediment rates in the Anzali Lagoon, Caspian Sea. J Radioanal Nucl Chem 322:319–330
4. Adegoke OS, Oyebamiji AS, Edet JJ, Osterloff PI, Ulu O, Adegoke OS, Oyebamiji AS, Edet JJ, Osterloff PI (eds) (2017) Elsevier, 386–394, https://doi.org/10.1016/B978-0-12-812161-0.00007-7
5. Akweetelela Ananias N, Kgabi M, Zivuku D, Mashauri (2022) Environmental radioactivity of groundwater and sediments in the Kuiseb. and Okavango-Omatako basins in Namibia
6. https://doi.org/10.1016/j.pce.2020.102911
7. Bastami KD, Neyestani MR, Shemirani F, Soltani F, Haghparast S, Akbari A (2015) Heavy metal pollution assessment in relation to sediment properties in the coastal sediments of the southern Caspian Sea. Mar Pollut Bull 92:237–243
8. Bonsignore M, Manta DS, Sharif, E.A.A.-T., D'Agostino F, Traina A, Quinci EM, Giaramita L, Monastero C, Benothman M, Sprovieri M (2018) Marine pollution in the Libyan coastal area: environmental and risk assessment. Mar Pollut Bull 128:340–352
9. Delbono I, Barsanti M, Schirone A, Conte F, Delfanti R (2016) 210Pb mass accumulation rates in the depositional area of the Magra River (Mediterranean Sea, Italy). Cont. Shelf Res 124:35–48
10. Fallah M, Jahangiri S, Janadeleh H, Kameli MA (2019) Distribution and risk assessment of radionuclides in river sediments along the Arvand River. Iran Microchem J 146:1090–1094. https://doi.org/10.1016/j.microc.2019.02.028
11. Fouskas F, Godelitsas A, Argyraki A, Pappa FK, Tsabaris C (2018) Metal concentrations and radioactivity in sediments at the northern coastal zone of Ikaria Island, eastern Mediterranean, Greece. J Radioanal Nucl Chem 317:55–68
12. Bonsignore M, Manta DS, Sharif, E.A.A.-T., D'Agostino F, Traina A, Quinci EM, Giaramita L, Monastero C, Benothman M, Sprovieri M (2018) Marine pollution in the Libyan coastal area: environmental and

risk assessment. Mar Pollut Bull 128:340–352

13. Delbono I, Barsanti M, Schirone A, Conte F, Delfanti R (2016) 210Pb mass accumulation rates in the depositional area of the Magra River (Mediterranean Sea, Italy). Cont. Shelf Res 124:35–48
14. Fallah M, Jahangiri S, Janadeleh H, Kameli MA (2019) Distribution and risk assessment of radionuclides in river sediments along the Arvand River. Iran Microchem J 146:1090–1094. https://doi.org/10.1016/j.microc.2019.02.028
15. Fouskas F, Godelitsas A, Argyraki A, Pappa FK, Tsabaris C (2018) Metal concentrations and radioactivity in sediments at the northern coastal zone of Ikaria Island, eastern Mediterranean, Greece. J Radioanal Nucl Chem 317:55–68
16. d'Almeida G, Kaki C, Adeoye J Benin and Western Nigeria Offshore Basins: A Stratigraphic Nomenclature Comparison.International Journal of Geosciences, 2016 7,177–188. doi: 10.4236/ijg.2016.72014
17. Graba NN, Ramli AT, Saleh MA, Sanusi SM, Gabdo HT (2018) Radiological mapping of Kelantan, Malaysia, using terrestrial radiation dose rate. Isot Environ Health Stud 52(3):214–218
18. How oil and water create a complex conflict in the Niger Delta. https://theconversation.com/how-oil-and-water-create-a-complex-conflict-in-the-niger-delta-135105 (Accessed on 19 May 2021).
19. Gu, Y.-G., Lin, Q., Huang, H.-H., Wang, L., Ning, J.-J., Du, F.-Y., 2017. Heavy metals in fish tissues/stomach contents in four marine wild commercially valuable fish species from the western continental shelf of South China Sea. Mar. Pollut. Bull. 114, 1125–1129
20. Hesham M.H. Zakaly , M.A.M. Uosif , Shams A.M. Issa, H.O. Tekin, Hashim Madkour, Mahmoud Tammam, Atef El-Taher, Gharam A. Alharshan, Mostafa Y. A. Mostafa, (2021). An extended assessment of natural radioactivity in the sediments of the mid-region of the Egyptian Red Sea coast, Marine Pollution Bulletin 171 (2021) 112658
21. Hurtado-Bermúdez, S., Valencia, J.M., Rivera-Silva, J., Mas, J.L., Aparicio, I., Santos, J.L., Alonso, E., 2019. Levels of radionuclide concentrations in benthic invertebrate species from the Balearic Islands, Western Mediterranean, during 2012–2018. Mar. Pollut. Bull. 149, 110519
22. Janadeleh, H., Jahangiri, S., Kameli, M.A., 2018a. Assessment of heavy metal pollution and ecological risk in marine sediments (a case study: Persian Gulf). Hum. Ecol. Risk Assess. An Int. J. 24, 2265–2274. https://doi.org/10.1080/ 10807039.2018.1443792.
23. Janadeleh, H., Kameli, M.A., Boazar, C., 2018b. Seasonal variations of metal pollution and distribution, sources, and ecological risk of polycyclic aromatic hydrocarbons (PAHs) in the sediment of the Al Hawizah wetland, Iran. Hum. Ecol. Risk Assess. An Int. J. 24, 886–903. https://doi.org/10.1080/10807039.2016.1277416
24. ICRP 1991. Recommendations of the International Commission on Radiological Protection 1990 (ICRP) Publication No. 60. Annals of the ICRP 21: 1-201.
25. IAEA (1996). Radiation protection and the safety of Radiation sources. International Atomic Energy Agency, Wagramerstrsse 5, A1400 Vienna. Austria. IAEA-RPSR-1 Rev 1

26. Jibiri N.N., I.C. Okeyode, Evaluation of radiological hazards in the sediments of Ogun River, South-Western Nigeria, Radiat. Phys. Chem. 81 (2012) 103–112
27. Mutiu, A. A.; Gbolahan, I.; Oluwaseyi, A. O.; Folashade, H. F.; Adeyemi, Y. A.; Taofeeq, A. A. and Adelowo, A. A. Water Quality Assessment of Iju River in Ogun State, Nigeria: Effect of Human Activities. *Journal Of Environmental Science. Toxicology and Food Technology*. **2013**, 6(3), 64-68.
28. Nyarko, E.; Botwe, B. O.; Ansong, J. E.; Delfanti, R.; Barsanti, M.; Schirone, A.; and Delbono, I. Determination of 210Pb, 226Ra and 137Cs in beach sands along the coastline of Ghana. *African Journal of Environmental Pollution and Health* 2011, 9, 17–23
29. Nour, H.E., El-Sorogy, A.S., El-Wahab, M.A., Nouh, E.S., Mohamaden, M., Al-Kahtany, K., 2019. Contamination and ecological risk assessment of heavy metals pollution from the Shalateen coastal sediments, Red Sea, Egypt. Mar. Pollut. Bull. 144, 167–172.
30. Omeje et al. Natural radioactivity concentration of 226Ra, Thorium-232, and Potassium-40 in commercial building materials and their lifetime cancer risk assessment in dwellers, human and ecological risk assessment, Int. J. **2018**, 24 (8), 214
31. Orosun, M. M.; Usikalu, M. R.; Oyewumi, K. J.; Achuka J. A. Radioactivity levels and transfer factor for granite mining field in Asa, North-central Nigeria. *Heliyon*. **2020**, 6(6), e04240. https://doi.org/10.1016/j.heliyon.2020.e04240
32. Orosun, M. M.; Oniku, A. S.; Adie, P.; Orosun, O. R.; Salawu, N. B.; Louis, H. Magnetic susceptibility measurement and heavy metal accid at an automobile station in Ilorin, North-Central Nigeria, *Environ. Res. Commun*. **2020,** 2, 015001. https://doi.org/10.1088/2515-7620/ab636a
33. Orosun, M. M., Oyewumi, K. J., Usikalu, M. R., Onumejor, C. A. (2020b). Dataset on radioactivity measurement of Beryllium mining field in Ifelodun and Gold mining field in Moro, Kwara State, North-central Nigeria. Data in Brief. 31, 105888. https://doi.org/10.1016/j.dib.2020.105888
34. Orosun M. M.; Tchokossa P.; Orosun R. O.; Akinyose F. C.; Ige S. O. Determination of Selected Heavy Metals and Human Health Risk Assessment in Fishes from Kiri Dam and River Gongola, Northeastern Nigeria. *J Phys Chem Biophys* **2016,** 6, 229. doi:10.4172/2161-0398.1000229.
35. Sugandhi, S., Joshi, V. M., & Ravi, P. (2014). Studies on natural and anthropogenic radionuclides in sediment and biota of Mumbai Harbour Bay. *Journal of Radioanalytical and Nuclear Chemistry*, 300(1),
36. Singh, P.K., Saxena, S., 2018. Towards developing a river health index. *Ecol. Indicat*. 85, 999-1011. https://doi.org/10.1016/j.ecolind.2017.11.059
37. Pappa, F.K., Tsabaris, C., Ioannidou, A., Patiris, D.L., Kaberi, H., Pashalidis, I. Eleftheriou, G., Androulakaki, E.G., Vlastou, R., 2016. Radioactivity and metal concentrations in marine sediments associated with mining activities in Ierissos Gulf, North Aegean Sea, Greece. Appl. Radiat. Isot. 116, 22–33
38. United Nations Scientific on the Effects of Radiation (UNSCEAR, 2000), Sources and effects of ionization radiation.

https://www.unscear.org/docs/publications/2000/UNSCEAR_2000_Report_Vol.I.pdf. (Accessed on 19 May 2021).

39. Uluturhan, E.; Kontaş, A.; Can E. Sediment concentrations of heavy metals in the Homa Lagoon (Eastern Aegean Sea): assessment of contamination and ecological risks. *Mar Pollut Bull* **2011**, 62, 1989–1997

Figures

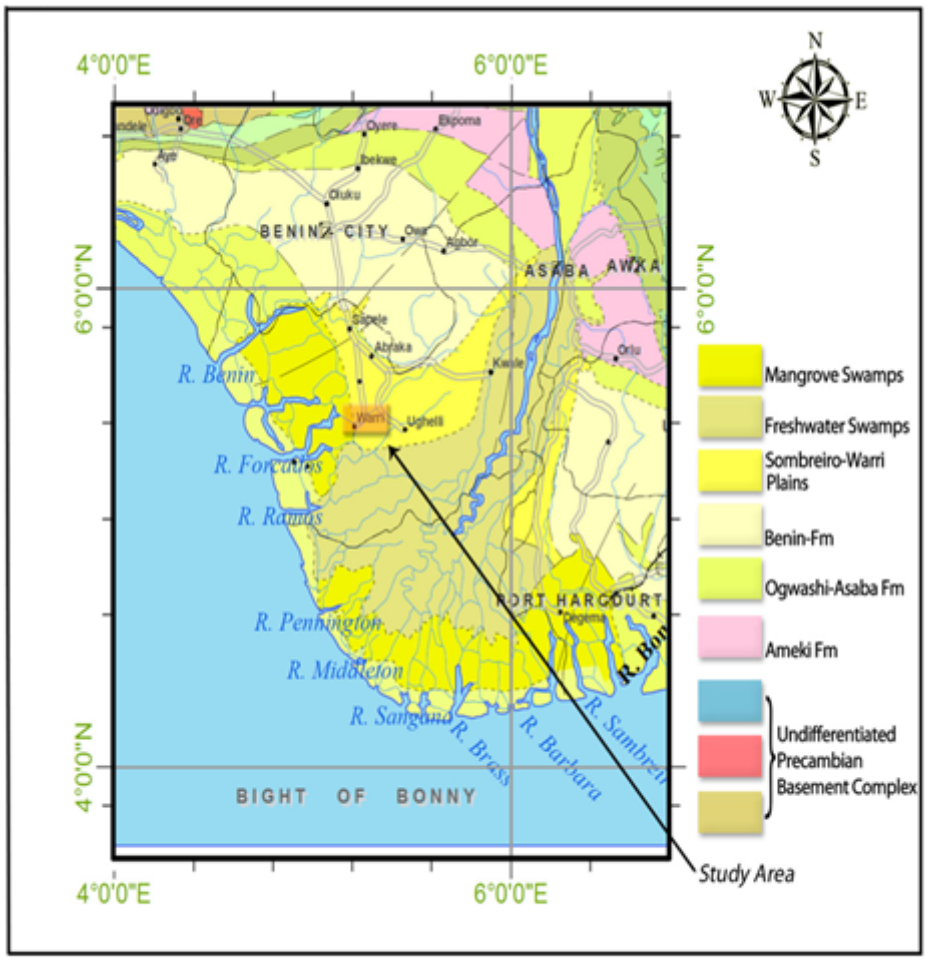

Figure 1

Geology of the study area (Source: NGGSA, 2004 and Irwin, 2015

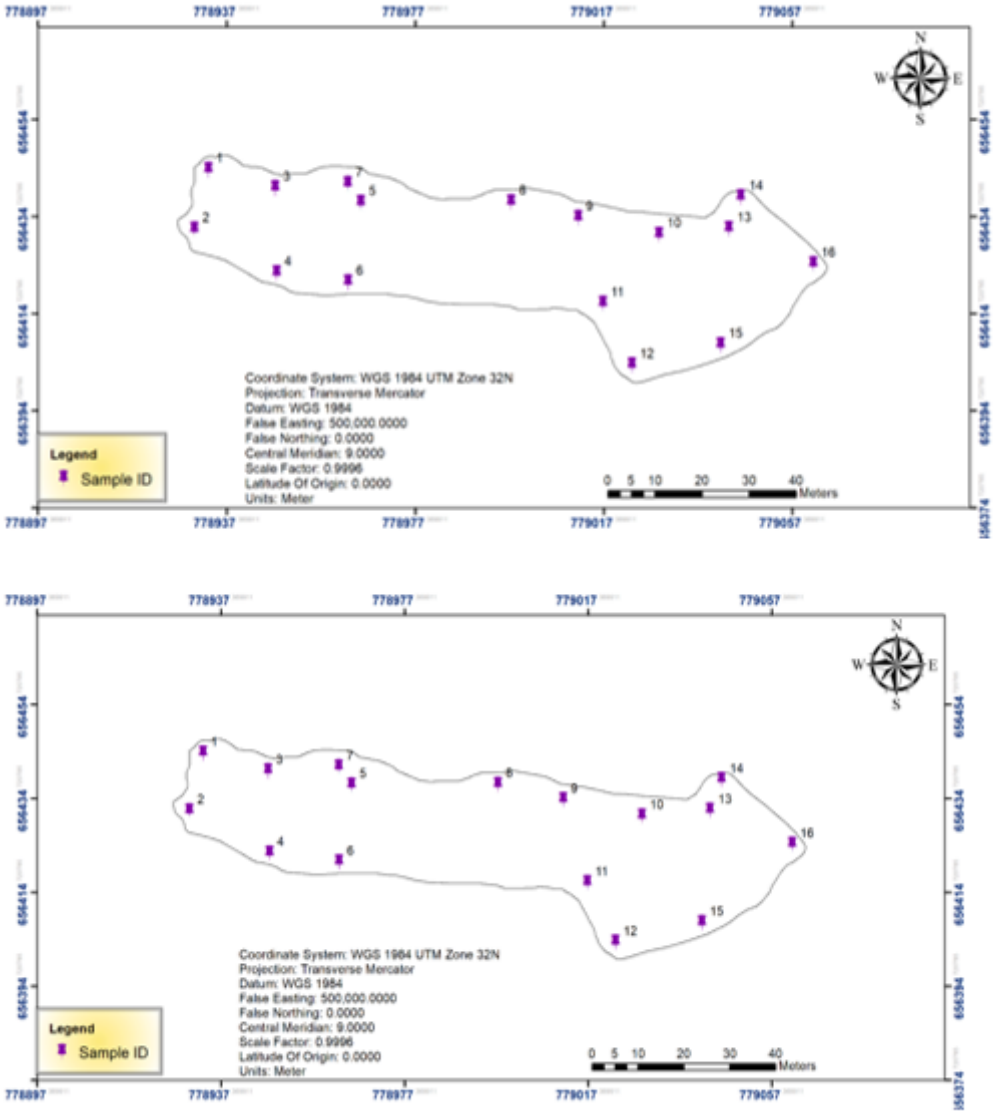

Figure 2

Sample collection points

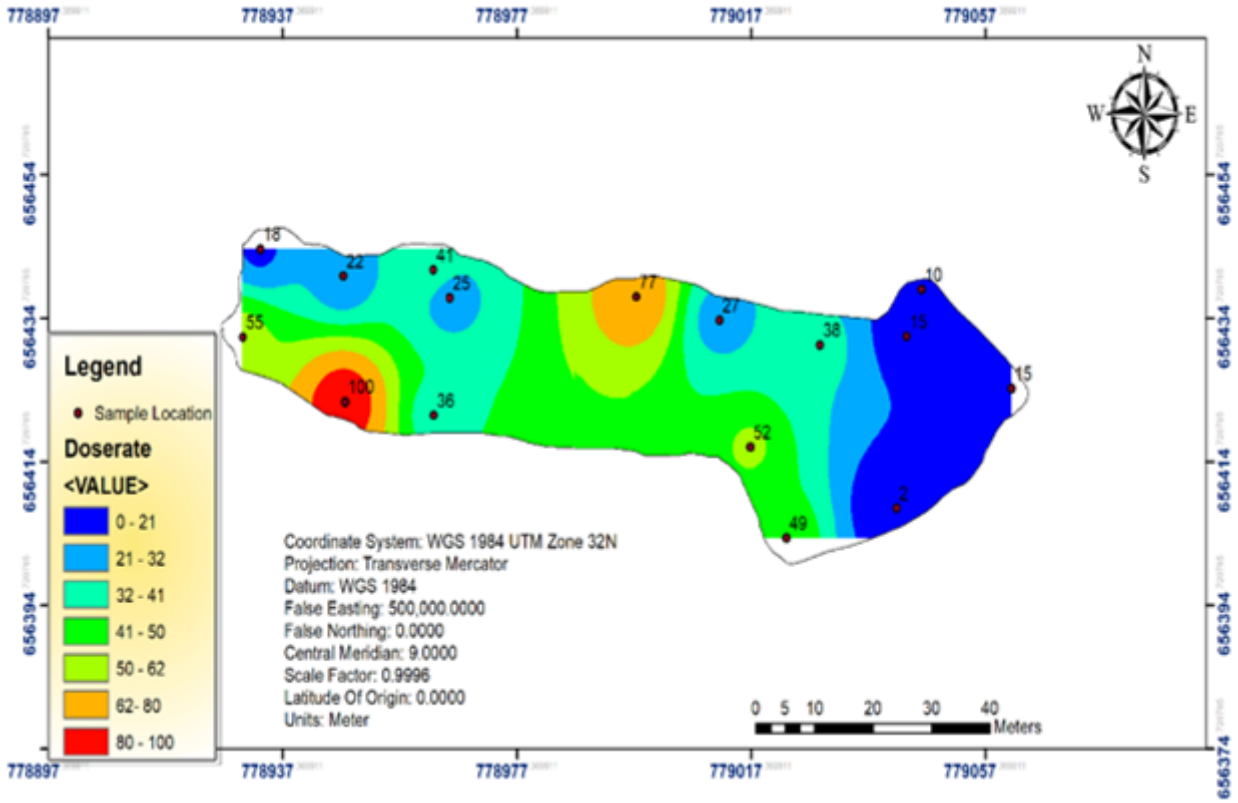

Figure 3

Spatial distribution of In-situ measured Dose rate

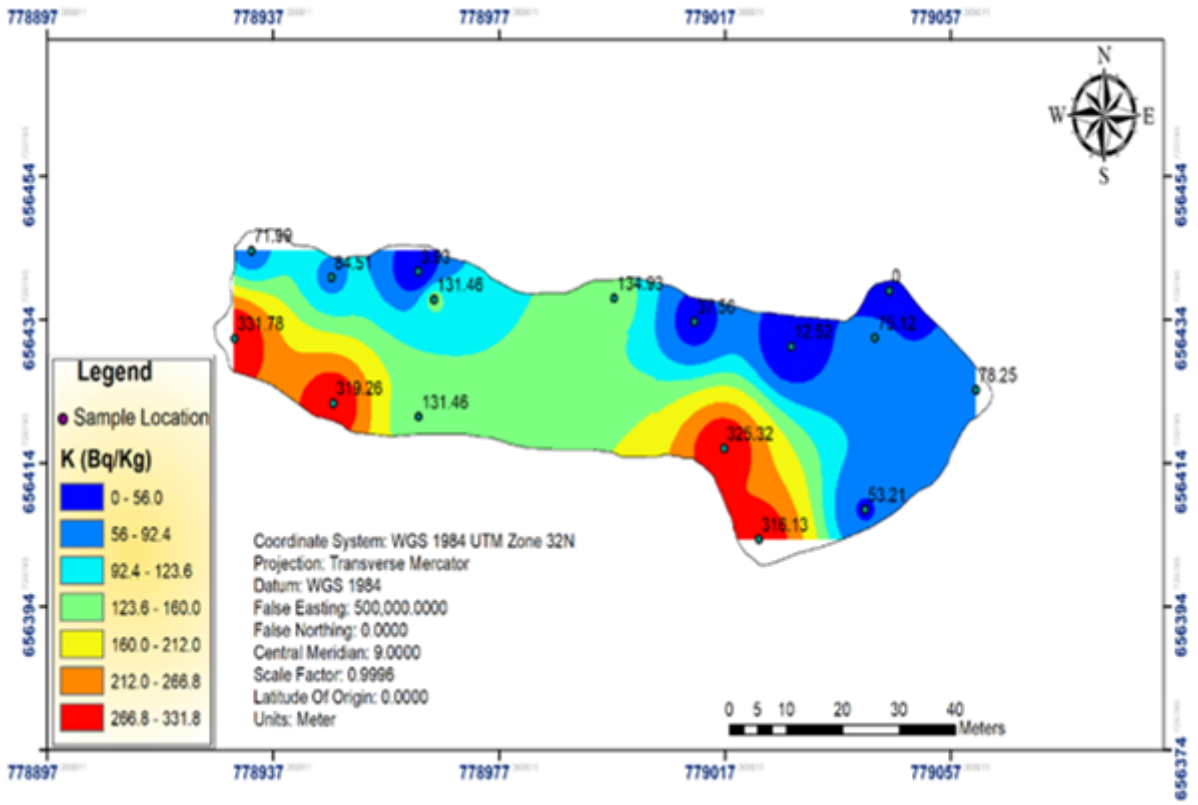

Figure 4

Spatial distribution of In-situ measured Activity concentration of Potassium-40

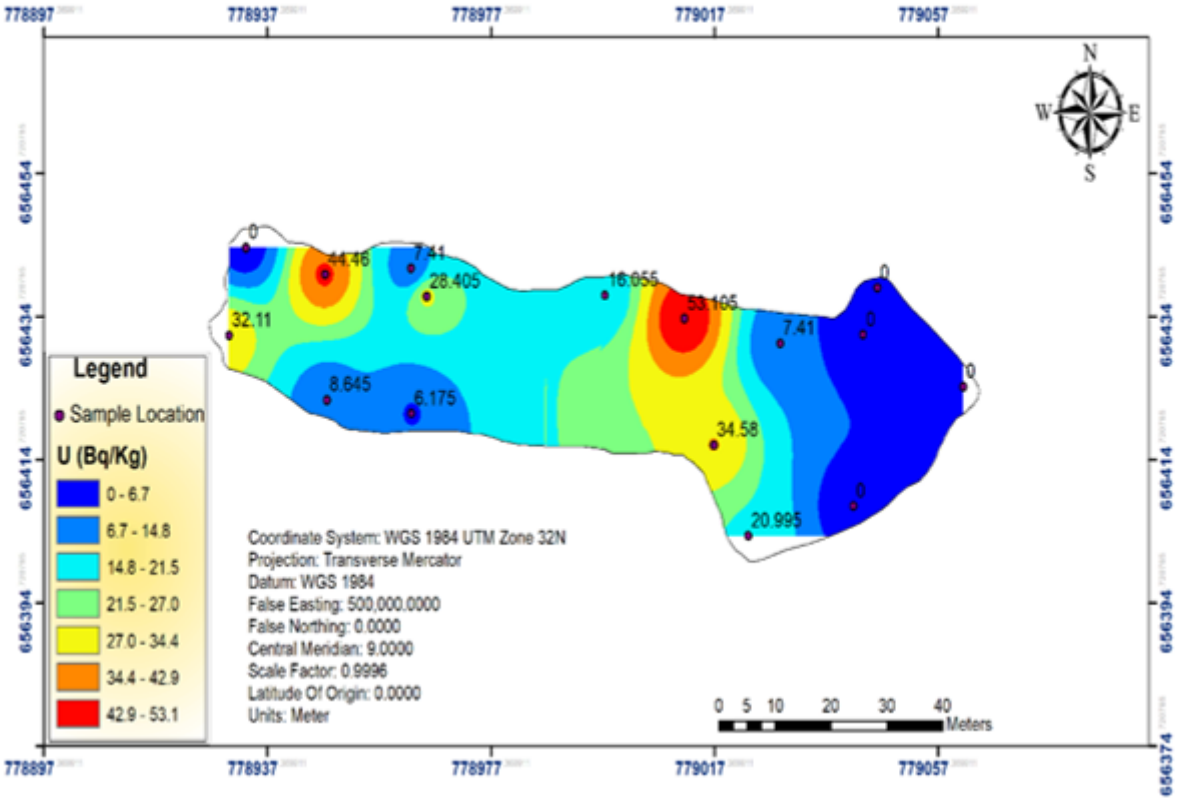

Figure 5

Spatial distribution of In-situ measured Activity concentration of Uranium-238.

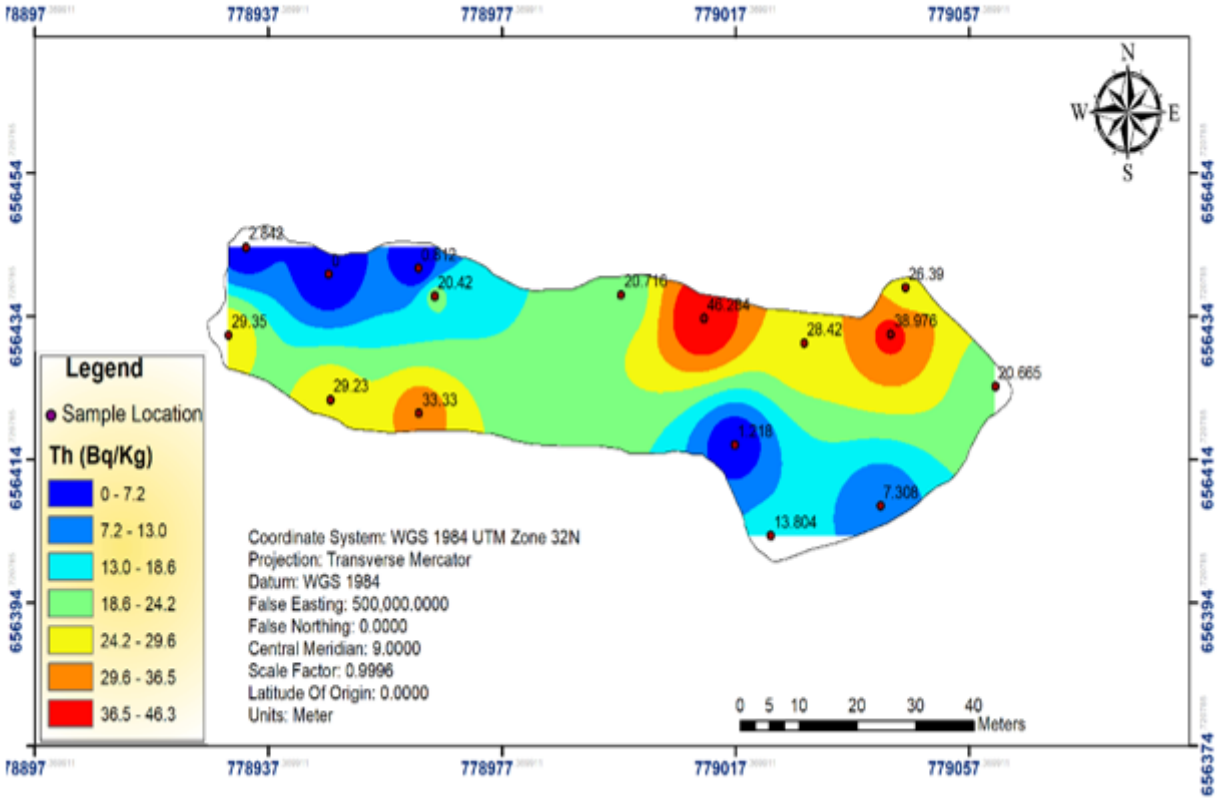

Figure 6

Spatial distribution of In-situ measured Activity concentration of Thorium-232

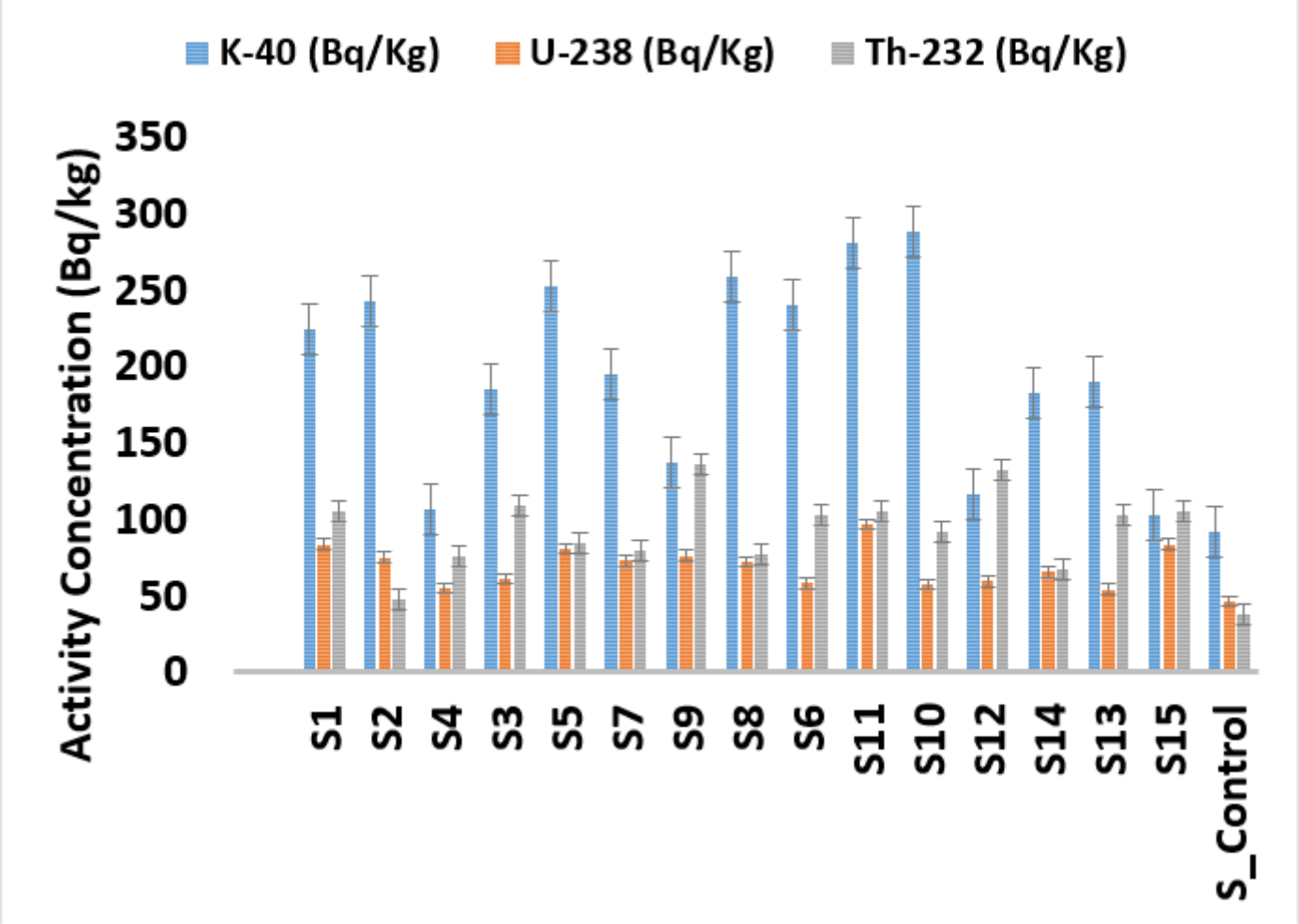

Figure 7

Activity concentration of Potassium-40, Uranium-238, and Thorium-232 in the sediment samples

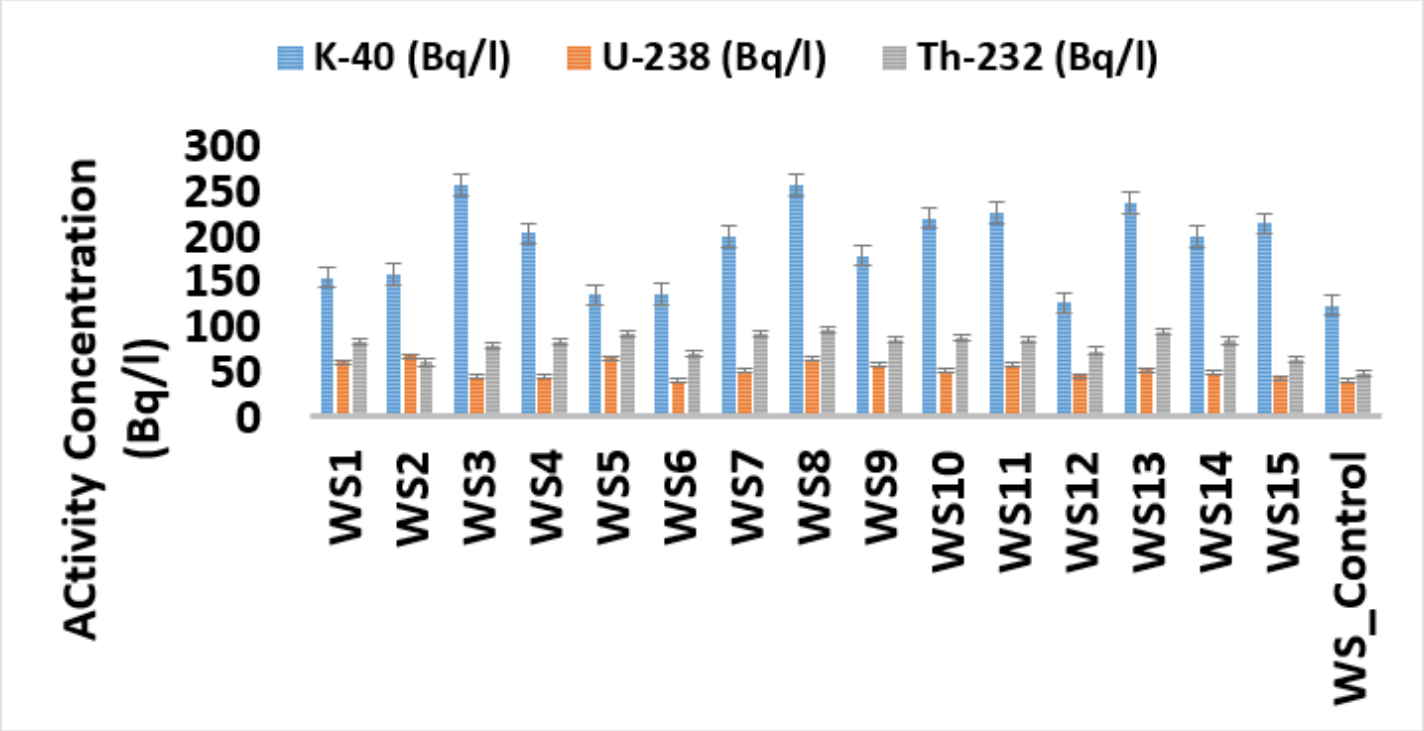

Figure 8

Activity concentration of Potassium-40, Uranium-238, and Thorium-232 in the water samples

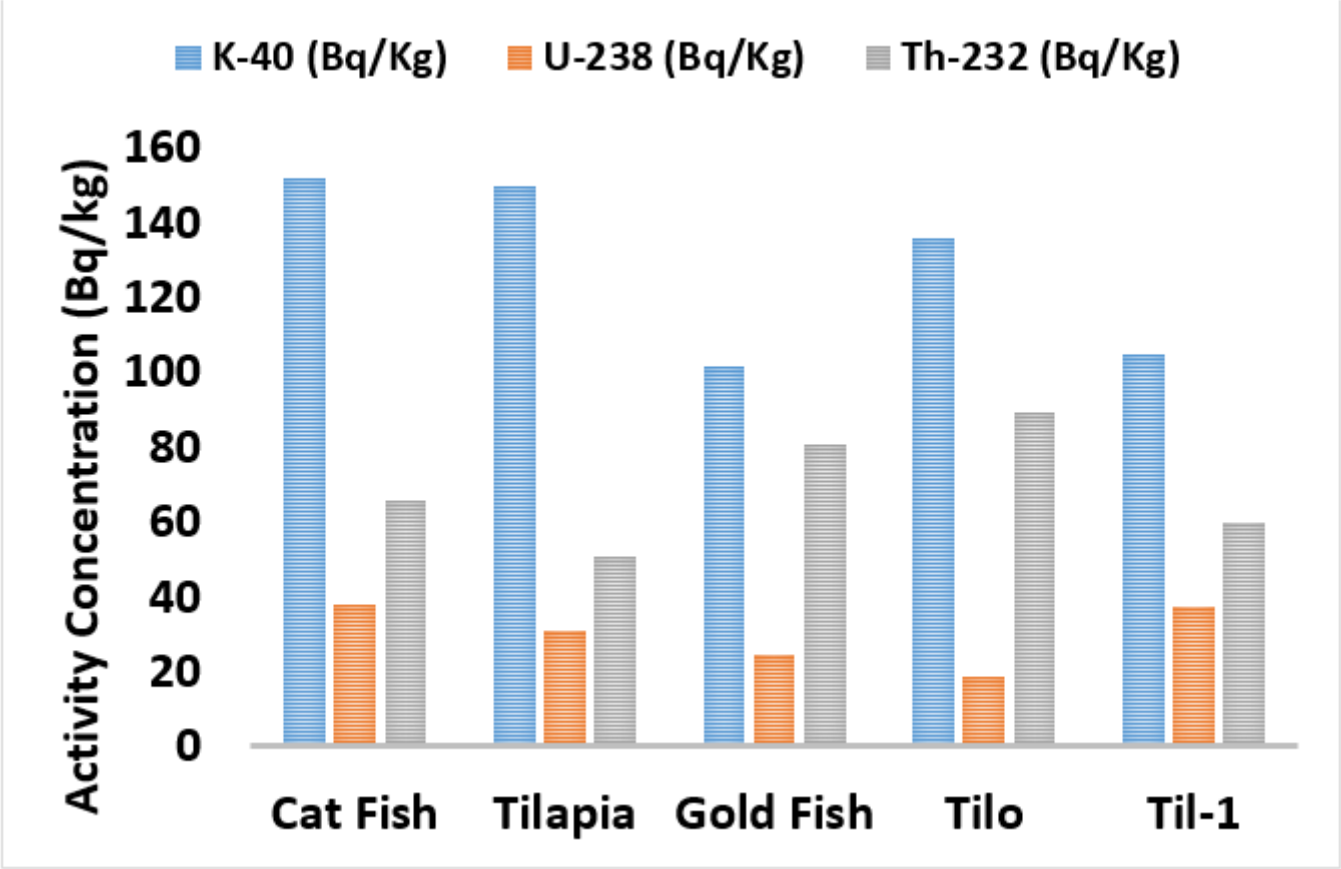

Figure 9

Activity concentration of Potassium-40, Uranium-238, and Thorium-232 in the Fish samples

Supplementary Files

This is a list of supplementary files associated with this preprint. Click to download.

- SupportingDocumentsforAchives.docx